AIP | Applied Physics Letters

Enhanced axial confinement in a monolithically integrated self-rolled-up SiNx vertical microring photonic coupler

Xin Yu, Lynford L. Goddard, Xiuling Li, and Xiaogang Chen

Citation: Applied Physics Letters **109**, 111104 (2016); doi: 10.1063/1.4962901
View online: http://dx.doi.org/10.1063/1.4962901
View Table of Contents: http://scitation.aip.org/content/aip/journal/apl/109/11?ver=pdfcov
Published by the AIP Publishing

Enhanced axial confinement in a monolithically integrated self-rolled-up SiN_x vertical microring photonic coupler

Xin Yu, Lynford L. Goddard, Xiuling Li, and Xiaogang Chen[a)]
Department of Electrical and Computer Engineering, Micro and Nanotechnology Laboratory, University of Illinois, Urbana, Illinois 61801, USA

(Received 20 July 2016; accepted 4 September 2016; published online 14 September 2016)

We report an efficient method to introduce enhanced axial confinement in the self-rolled-up SiN_x vertical microtube coupler by depositing a thin layer of high refractive index material strip within the coupling section and effectively forming a vertical microring. Three times wider mode spacing is observed in such a vertical microring coupler monolithically integrated with a silicon nitride ridge waveguide as compared to the one without such axial confinement. More importantly, single mode operation within the telecomm C-band and S-band is achieved. *Published by AIP Publishing.* [http://dx.doi.org/10.1063/1.4962901]

The self-rolled-up microtube has been demonstrated to be a versatile device platform, which has found application in a number of areas including nanophotonics,[1–7] microelectronics,[8] chemical and biological sensing,[9–11] and intelligent synthetic neural circuits.[12] Because the microtube is a three dimensional (3D) structure readily fabricated using two dimensional processing technology, it may serve naturally as a component in 3D-integrated devices. We had previously demonstrated a vertical microtube coupler (VμTC) monolithically integrated with planar ridge waveguides in silicon photonic platform to achieve 3D photonic coupling and observed greatly enhanced coupling between the microtube and the underlying ridge waveguide.[1,13] A similar result was reported independently by another research group shortly thereafter.[2] One limitation of the VμTC used in previous experiments is that it supports many modes within the telecommunication C-band because of poor axial confinement. For example, we found multiple resonant coupling peaks, which is not desirable for wavelength division multiplexing (WDM) switches. In order to increase the mode spacing of this 3D photonic coupler and to achieve single mode operation within the C-band, we propose efficient axial confinement in the microtube to suppress the higher order modes. Axial confinement in self-rolled-up microtubes had been studied both theoretically and experimentally by a couple of research groups.[14–17] In all these previous cases, the axial confinement was introduced by a specially designed geometrical shape of a section of the microtube. After being rolled up, the microtube wall will have different thicknesses at different axial locations. The different wall thicknesses result in a slightly varying effective refractive index of the supported whispering gallery modes (WGMs) along the axial direction of the microtube. When a parabolic shape is used, the effective index of the WGM at the center of the parabola will be the highest and decrease adiabatically along both sides. However, the refractive index change due to different wall thicknesses is very small; hence, the axial confinement is rather weak. In this paper, we present our experimental endeavor to incorporate a different axial confinement scheme in the monolithically integrated vertical microtube (VμT) to form a vertical microring (VμR) resonator and demonstrate 3 times wider mode spacing than the microtube based vertical photonic coupler and the potential to achieve a higher Q-factor.

The method that we used to introduce the axial confinement in the VμT is to deposit a thin strip of high refractive index material on the planar microtube pattern before it is rolled-up. The high index strip within the microtube increases the effective refractive index locally. Therefore, the refractive index profile along the axial direction exhibits a discontinuity similar to a step-index waveguide, which will help to confine the electromagnetic field within the high refractive index region and effectively form a vertical microring coupler (VμRC).

In our experiment, we choose to use amorphous silicon (*a*-Si) as the high refractive index material on top of the SiN_x bilayer film as illustrated in Fig. 1(a). The top two figures in Fig. 1(a) show the two planar patterns used to form the VμR resonator. The bottom two are the corresponding cross-sectional view of the devices along the axial direction after being rolled-up. The fabrication process of the VμRC monolithically integrated on top of the ridge waveguide is similar to that of the VμTC as reported in Ref. 1. After the waveguide formation and surface planarization, a 20 nm germanium (Ge) sacrificial layer, low frequency (LF) SiN_x, and high frequency (HF) SiN_x were deposited sequentially by a dual-frequency plasma enhanced chemical vapor deposition (PECVD). Subsequently, the *a*-Si strip was deposited on the HF SiN_x layer by lift-off process to form the axial confinement structure, and its geometric dimensions were defined by an e-beam evaporator and a contact optical lithography. The strip was placed directly on top of the Si_3N_4 ridge waveguide to facilitate photonic coupling. Fig. 1(b) shows the refractive indices of all the materials consisted in the VμRC structure. The values are measured by a J. A. Woollam Co. variable-angle spectroscopic ellipsometer. The measured refractive index of the *a*-Si thin film is more than 30% higher than the average refractive index of the SiN_x bilayer.

We fabricated the two types of VμRs illustrated in Fig. 1(a). In both cases, the thicknesses of the LF and the HF

[a)]Author to whom correspondence should be addressed. Electronic mail: oxgchen@illinois.edu

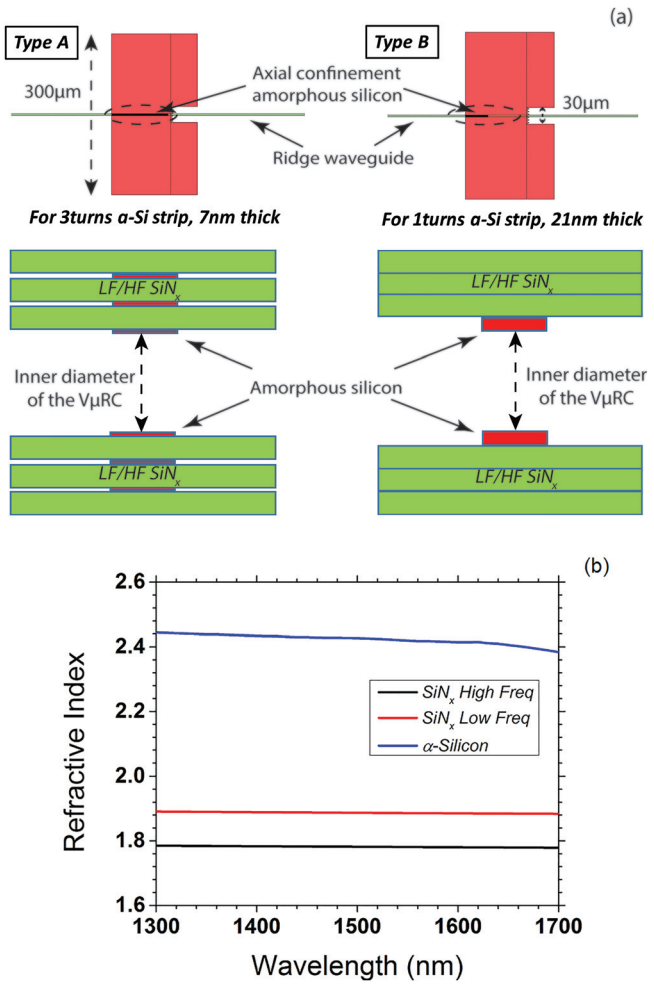

FIG. 1. (a) Two planar microtube patterns (up) and the corresponding cross-sectional view of the microtube structures along the axial direction (bottom) after being rolled-up. (b) The refractive index of the materials measured by ellipsometry.

SiN_x layer are 20 nm and 40 nm, respectively. The residual stress of LF layer is −880 MPa and that of the HF layer is 340 MPa. The width of the *a*-Si strip in both devices is 3 μm, which matches with the width of the underlying ridge waveguide. Fig. 2 shows the two types of VμR resonator patterns before and after the self-rolled-up process. The thickness and length of the *a*-Si strip of the device on the top (Type-A) of Fig. 2 are 7 nm and 75 μm, while those at the lower one (Type-B) are 21 nm and 25 μm, respectively. Once the Ge sacrificial layer was selectively etched away from the left trench to the right terminal point, the *a*-Si strip was scrolled into a VμR wrapped by the SiN_x bilayer as a rolling vehicle. After rolling, both of the devices have 3 full revolving turns. Therefore, the total thickness of the *a*-Si strip at any given axial location is the same. The two insets in Fig. 2 are the scanning electron microscopy (SEM) images of the two types of the VμR resonator integrated directly on top of the Si_3N_4 ridge waveguide. The nominal diameter of the tubes is 8 μm.

Similar to the VμTC and ridge waveguide integration, the vertical coupling distance can be controlled by the thickness of the spin on glass (SOG) planarization layer and the number of turns of the two extended pedestals on both sides of the microtube pattern. For the VμRC devices we used in our experiment, the total gap for coupling is 110 nm, including a 50 nm SOG layer and a 1 full turn of SiN_x tube (20 nm LF + 40 nm HF). We choose this coupling distance because it gave us the best coupling result in previous VμTC coupling experiments.

To characterize the VμRC devices, we use the same experimental setup as that reported in Ref. 1. The wavelength of the input tunable laser source spans from 1450 nm to 1590 nm, which covers the entire telecommunication S-band (1460 nm–1530 nm) and C-band (1530 nm–1565 nm). The laser output passes through an optical isolator, a polarization controller, and a polarizer to ensure that the input light to the ridge waveguide is linearly polarized. It is then coupled into and collected from the ridge waveguide using tapered fiber lens to improve coupling efficiency. The coupling loss is typically 4.0 dB/facet. The transmitted light passes through an optical coupler and is sent to a photo-detector and an optical power meter.

Figure 3 shows the typical transmission spectra of two VμRC devices of Type-A. The microtube patterns, the thickness, and the height of the *a*-Si strip are the same. The devices are fabricated simultaneously. The only difference comes from the width of the *a*-Si strip. For Device 1, the width is 3 μm, matched with the width of the underlying ridge waveguide, while for Device 2, it is 6 μm, twice as wide as the underlying ridge waveguide. Resonance coupling between the VμRC and the ridge waveguide can be clearly identified by the discrete valleys in the transmission spectra for both devices. One may notice that the resonance coupling peaks, i.e., the valley in the transmission spectrum, of Device 2 (blue curve) exhibit larger full width half maximum (FWHM) around 6.0 nm and higher extinction ratio of 5.5 dB, while those of the Device 1 exhibit smaller FWHM around 2.0 nm and smaller extinction ratio of 2.1 dB. We found a larger dip in the transmission spectrum of Device 2, which indicates that Device 2 is closer to being critically coupled for the gap used in our experiment. Furthermore, in Fig. 3, one may notice that there is a small dip (~1 dB) lying between the adjacent major resonance valleys at around 1471 nm and 1523 nm for Device 2. This might indicate that the wider VμRC supports more than one axial mode. In order to achieve true single mode operation, one may need to use a VμRC with tight axial confinement that is also mode matched to the bus waveguide, such as the 3 μm wide strip in Device 1. The larger FWHM and lower loaded Q-factor in Device 2 could be attributed to the fact that the width of the high refractive index material in Device 2 is much larger than that in Device 1. The scattering from the fundamental mode into modes with axial mode number greater than 1 in the VμRC due to mode mismatch at the microring to bus waveguide coupler represents an extra loss mechanism for light in the 6 μm microring. As a result, the loaded Q-factor of Device 2 is correspondingly lower.

The most important difference between the transmission spectra obtained from these VμRCs and the ones obtained from a VμTC of similar size is the increased mode spacing. In our previous publication, the average mode spacing for the VμTC was about 17 nm.[1] After we introduced the axial confinement, the mode spacing of the VμRC is about 52 nm, which is 3 times larger. Furthermore, we noticed that the two resonance coupling wavelengths in Device 1's spectrum fell individually into the S-band and C-band. Therefore, we

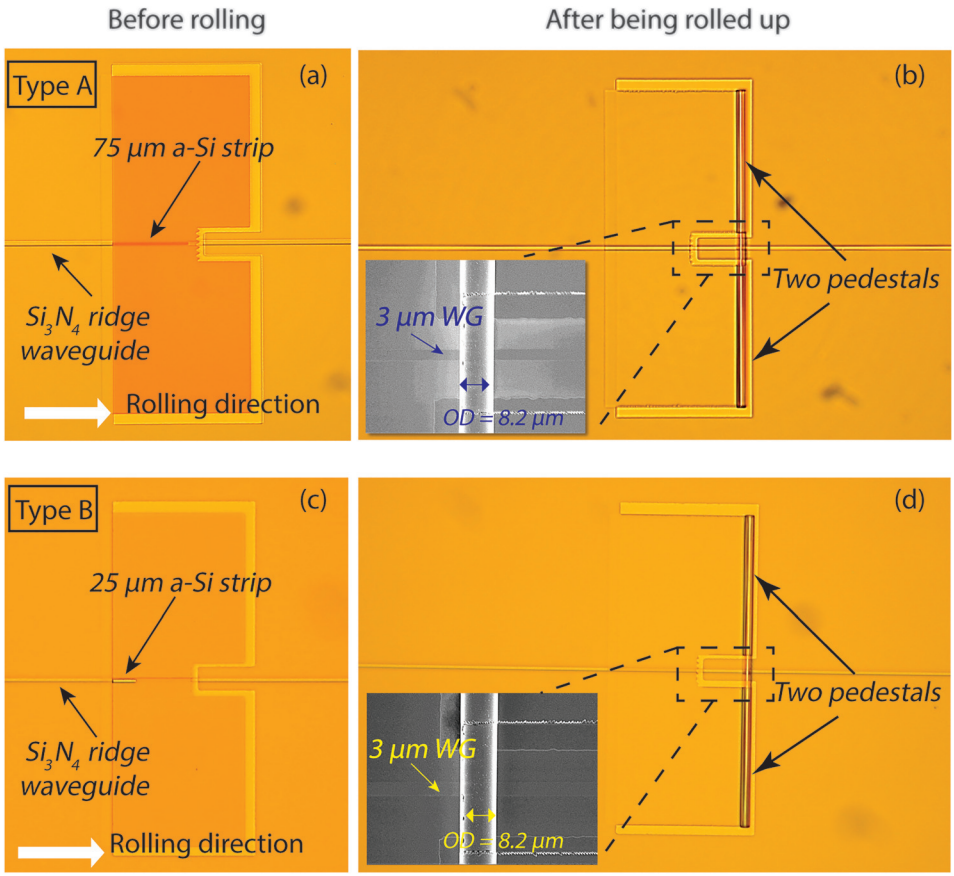

FIG. 2. The optical microscope images of the monolithically integrated Type-A and Type-B VμRC patterns on top of a ridge waveguide before (a), (c) and after self-rolling (b), (d), respectively. The insets in (b) and (d) are the SEM images of the VμRCs after their formation.

achieved single mode coupling within each band, which could greatly suppress the crosstalk between different wavelength channels. This is a very much desirable feature for using the VμRC as a WDM switch in a 3D photonic integrated system.

The transmission spectrum of a VμRC of Type-B is shown by the blue solid curve in Fig. 4. We may also identify two resonant coupling wavelengths of the VμRC located at 1480.8 nm and 1535.2 nm. The transmission spectrum of a Type-A VμRC with the same structural parameters (the dimensions of the microtube and the total thickness and the width of the *a*-Si layer) is also shown in the red dashed curve as a comparison. The mode spacing of this Type-B VμRC is comparable to that of the Type-A VμRC. One may notice that the FWHM of the resonant peak for the Type-B VμRC is much larger than that of the Type-A VμRC. We believe that this can be explained by the structural difference

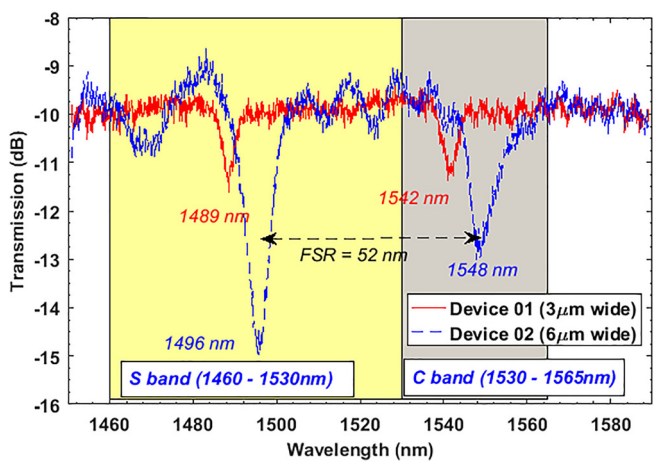

FIG. 3. The transmission spectra obtained from a ridge waveguide coupled to two different Type-A VμRCs. The red solid curve corresponds to the result obtained from a VμRC with 3 μm-wide *a*-Si strip. The blue dashed curve corresponds to the result obtained from a VμRC with 6 μm-wide *a*-Si strip. In both cases, the VμRC exhibits a 3× wider mode spacing than the previously reported VμTC with the same inner diameter. The free spectral range (FSR) of the VμRC is 52 nm. Additionally, we may notice that the 3 μm-wide *a*-Si strip VμRC supports only one resonant coupling mode within the telecommunication S-band and C-band.

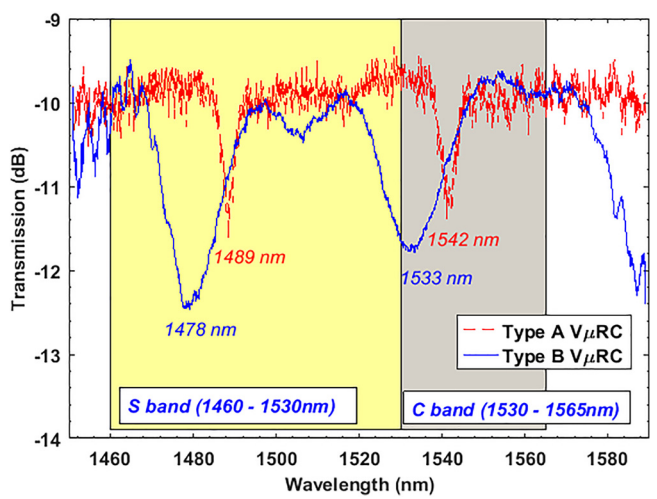

FIG. 4. The transmission spectra obtained from a ridge waveguide coupled to a Type-A (red dashed) and a Type B (blue solid) VμRC, as defined in Fig. 1(a). Both of the VμRCs contain a 3 μm-wide and total of 21 nm thick *a*-Si strip. The structural parameters of the enclosing microtube are the same.

between the Type-A and the Type B VμRCs. As shown in Fig. 1(a), the *a*-Si strip in the Type-A VμRC is distributed between each SiN_x microtube layer, whereas in the Type-B VμRC, the high index *a*-Si strip is concentrated in the inner diameter. Thus, the *a*-Si ring of the Type-B VμRC has higher bending loss and lower loaded Q-factor due to its smaller effective radius as compared to that of the Type-A VμRC. We would like to stress that the results presented in both Figs. 3 and 4 are typical results commonly observed in a group of similar devices fabricated using the same process.

To verify our experimental observation, we performed mode analysis simulations using COMSOL Multiphysics. Figures 5(a), 5(b), and 5(c) show zoomed-in views of the electric field profiles for the fundamental mode of the 3 μm wide Type-A, 3 μm wide Type-B, and 6 μm wide Type-A VμRCs, respectively. Comparing Figs. 5(a) and 5(b), we see that as expected, the field for the Type-B VμRC is confined closer to the inner radius than for the Type-A VμRC. Consequently, the extracted bending loss was much higher for Type-B (442 dB/cm) compared to Type-A (296 dB/cm). This explains most but not all of the observed difference in FWHM. Because the tube bending radius is small, the loss and FWHM are very sensitive to device geometry and although the total volume of *a*-Si is the same, the difference in the thickness and length may have affected the rolling properties of the 3 μm wide Type-A and Type-B VμRCs differently. Comparing Figs. 5(a) and 5(c), we see that the mode width for the 6 μm wide Type-A VμRC is about double that for the 3 μm wide Type-A VμRC. Therefore, the mode profile for the 6 μm wide VμRC is not matched to the profile of the mode travelling in the 3 μm bus waveguide underneath, which introduces scattering losses for light circulating in the VμRC. The second order mode is shown in Fig. 5(d). The simulations showed that the 3 μm wide VμRC is quasi-single mode: higher order axial modes exist, but they are not easily excited because the mode profiles match and moreover their loss is several times larger than that of the fundamental mode. In summary, we believe the 3 μm Type-A VμRC is a good design for WDM couplers in 3D photonic integration.

The self-rolled-up micro resonator is intrinsically a strained structure. Unlike bulk silicon, which does not exhibit a linear electro-optical effect due to the inverse symmetry of the crystalline structure, strained silicon has been reported to show second order nonlinear coefficient as high as $\chi^{(2)} = 122$ pm/V and an induced effective index change of $\Delta n_{Si} = 2.4 \times 10^{-5}$ at applied voltage of 30 V across a 10 μm gap.[18] In the VμRC we developed, it is relatively straightforward to introduce two electrodes side by side with the *a*-Si. The fabrication process of such a device is entirely compatible with the one we used to monolithically integrate the VμRC with a ridge waveguide and the CMOS processing

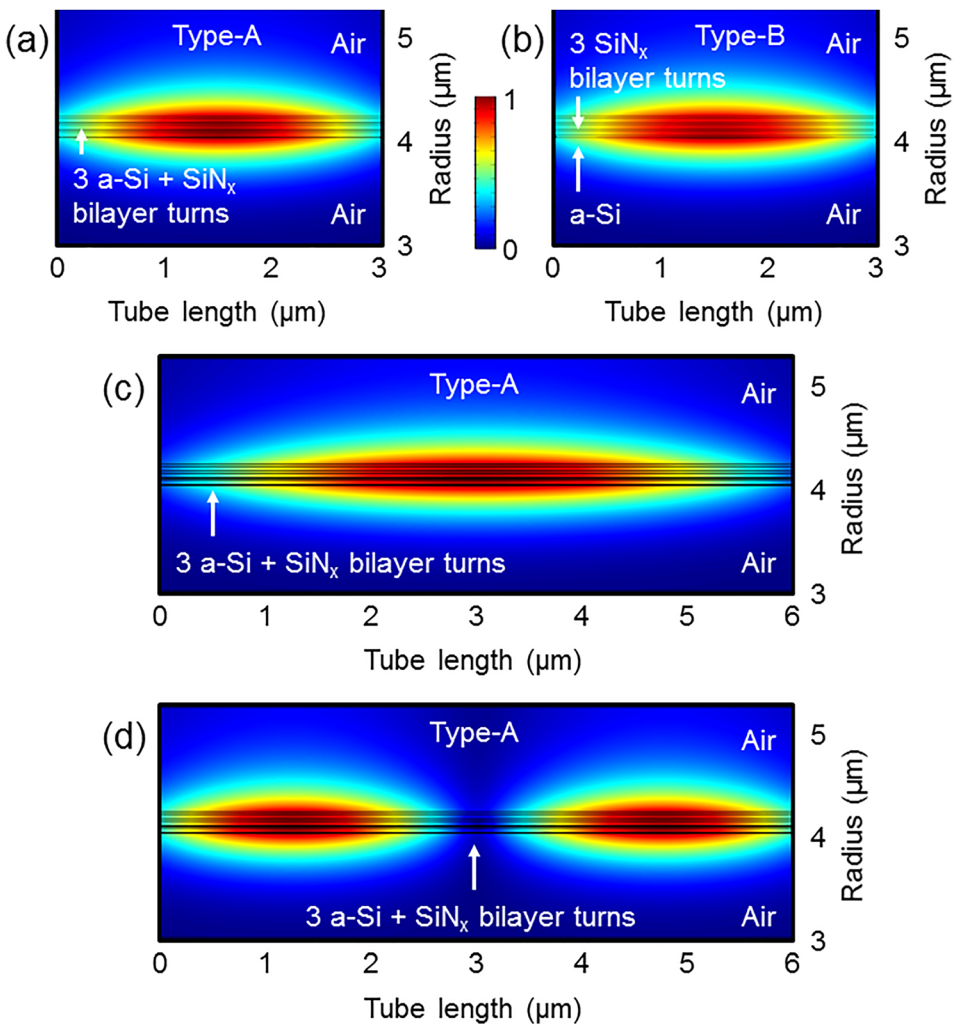

FIG. 5. Zoomed-in view of the electric field mode profile for the fundamental mode of the (a) 3 μm wide Type-A, (b) 3 μm wide Type-B, and (c) 6 μm wide Type-A VμRCs. (d) Second order axial mode profile of the 6 μm wide Type-A VμRC.

technology. Thus, it represents a potentially viable route to the development of an actively and electronically modulated VμRC.

In this paper, we presented an experimental study of introducing efficient axial confinement to the self-rolled-up microtube using deposited *a*-Si strip in the middle of the coupling section of the VμTC, which effectively formed a vertical microring structure. Similar to its predecessor, the VμRC can be monolithically integrated directly on top of a planar ridge waveguide. Resonant coupling between the VμRC and the ridge waveguide was observed experimentally using two types of the VμRC. One important improvement of the VμRC is that we achieved 3 times larger mode spacing than the VμTC of the same inner diameter and the same wall thickness. Moreover, we experimentally demonstrated single mode coupling within the technically important telecommunication S-band and C-band. It brings us one step closer to utilizing the VμRC as a vertical WDM coupler for 3D photonic integration. One additional advantage of the axial confinement scheme introduced in this paper is that it opens the potential to the further development of actively and electronically tunable VμRCs.

This work was carried out in part at the Micro and Nanotechnology Laboratory and at the Frederick Seitz Materials Research Laboratory Central Research Facilities, University of Illinois. The authors sincerely thank Dr. Julio Soares from the Materials Research Laboratory for his help on collecting the ellipsometry data. X.C. acknowledges financial support from the startup fund provided by the University of Illinois. X.L. acknowledges financial support by the U.S. Department of Energy, Office of Basic Energy Sciences, Division of Materials Sciences and Engineering under Award No. DE-FG0207ER46471. L.L.G. acknowledges financial support from NSF CAREER Award No. ECCS-1055941 with matching funds from the University of Illinois.

[1]X. Yu, E. Arbabi, L. Goddard, X. Li, and X. Chen, Appl. Phys. Lett. **107**(3), 031102 (2015).
[2]A. Madani, M. Kleinert, D. Stolarek, L. Zimmermann, L. B. Ma, and O. G. Schmidt, Opt. Lett. **40**(16), 3826 (2015).
[3]M. H. T. Dastjerdi, M. Djavid, and Z. Mi, Appl. Phys. Lett. **106**(2), 021114 (2015).
[4]B. Ciftcioglu, R. Berman, S. Wang, J. Y. Hu, I. Savidis, M. Jain, D. Moore, M. Huang, E. G. Friedman, G. Wicks, and H. Wu, Opt. Express **20**(4), 4331 (2012).
[5]Z. Mi, F. Li, Y. L. Chang, and J. L. Wang, ECS Trans. **28**(3), 285 (2010).
[6]S. Böttner, S. Li, M. R. Jorgensen, and O. G. Schmidt, Appl. Phys. Lett. **102**(25), 251119 (2013).
[7]X. G. Chen, Opt. Express **22**(13), 16363 (2014).
[8]X. Yu, W. Huang, M. Y. Li, T. M. Comberiate, S. B. Gong, J. E. Schutt-Aine, and X. Li, Sci. Rep. - Uk. **5**, 9661 (2015).
[9]V. A. B. Quinones, L. B. Ma, S. L. Li, M. Jorgensen, S. Kiravittaya, and O. G. Schmidt, Appl. Phys. Lett. **101**(15), 151107 (2012).
[10]E. J. Smith, S. Schulze, S. Kiravittaya, Y. Mei, S. Sanchez, and O. G. Schmidt, Nano Lett. **11**(10), 4037 (2011).
[11]G. S. Huang, V. A. B. Quinones, F. Ding, S. Kiravittaya, Y. F. Mei, and O. G. Schmidt, ACS Nano **4**(6), 3123 (2010).
[12]P. Froeter, Y. Huang, O. V. Cangellaris, W. Huang, E. W. Dent, M. U. Gillette, J. C. Williams, and X. Li, ACS Nano **8**(11), 11108 (2014).
[13]X. Yu, E. Arbabi, X. Li, L. Goddard, and X. Chen, CLEO: 2015 OSA Technical Digest, **SF1H.8**, San Jose, California, 2015.
[14]C. Strelow, C. M. Schultz, H. Rehberg, M. Sauer, H. Welsch, A. Stemmann, C. Heyn, D. Heitmann, and T. Kipp, Phys. Rev. B **85**(15), 155329 (2012).
[15]Ch. Strelow, H. Rehberg, C. M. Schultz, H. Welsch, Ch. Heyn, D. Heitmann, and T. Kipp, Phys. Rev. Lett. **101**(12), 127403 (2008).
[16]S. L. Li, L. B. Ma, H. L. Zhen, M. R. Jorgensen, S. Kiravittaya, and O. G. Schmidt, Appl. Phys. Lett. **101**(23), 231106 (2012).
[17]F. Li, S. Vicknesh, and Z. Mi, Electron. Lett. **45**(12), 645 (2009).
[18]B. Chmielak, M. Waldow, C. Matheisen, C. Ripperda, J. Bolten, T. Wahlbrink, M. Nagel, F. Merget, and H. Kurz, Opt. Express **19**(18), 17212 (2011).